Journal of Materials Chemistry A

Accepted Manuscript

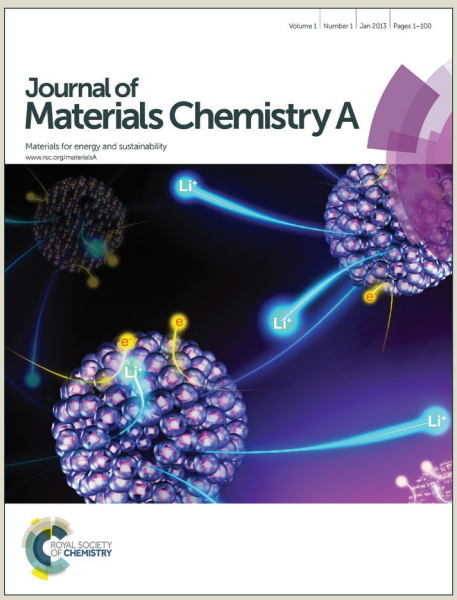

ROYAL SOCIETY OF CHEMISTRY

www.rsc.org/materialsA

Cite this: DOI: 10.1039/c0xx00000x

www.rsc.org/xxxxxx

ARTICLE TYPE

Highly Efficient Light-Harvesting Ruthenium Sensitizers for Dye-Sensitized Solar Cells Featuring Triphenylamine Donor Antenna

Kun Cao,[a] Jianfeng Lu,[a] Jin Cui,[a] Yan Shen,[a] Wei Chen,[a] Getachew Alemu,[a] Zhong Wang,[a] Huailiang Yuan,[a] Jie Xu,*[b] Mingkui Wang*[a] and Yibing Cheng[c]

Received (in XXX, XXX) Xth XXXXXXXXX 20XX, Accepted Xth XXXXXXXXX 20XX
DOI: 10.1039/b000000x

Two new heteroleptic ruthenium complexes, coded as KW1 and KW2, featuring with triphenylamine electron-donating antennas, have been synthesized and used in dye-sensitized solar cells (DSSCs). Compared to the reference dye Z907, these new dyes exhibit broad absorption and efficient light harvesting properties. Particularly the KW2 dye exhibits a low-energy metal-ligand charge transfer band centred at 554 nm with high molar extinction coefficient of 2.43×10^4 M^{-1} cm^{-1} arising from an extended conjugation in the donor-antenna ligand. Photovoltaic devices using these sensitizers in conjunction with a volatile electrolyte show high photovoltaic conversion efficiencies of ~10.7% under full sunlight irradiation (AM 1.5G, 100 mW cm^{-2}). This efficiency is nearly 20% higher than that of the Z907-based reference device, which is attributed to a largely improved short circuit current. The distinctly effect of different donor-antennas incorporated in the ancillary ligands on the primary photovoltaic parameters in these devices are investigated with transient photoelectrical decays and impedance spectroscopy measurements. The devices utilizing these highly efficient light harvesting ruthenium sensitizers featuring triphenylamine donor antenna in combination with low volatility electrolyte exhibit good durability during the accelerated tests (60 ^oC for 1000 h in a solar simulator, 100 mW cm^{-2}).

Introduction

Dye-sensitized solar cells (DSSCs) have received considerable attention due to their relatively low production cost and other attractive features, such as transparency and flexibility.[1] Photo-sensitizer is one of the most important components of this type device, which is responsible for the light harvesting and electron injection. Various photo-sensitizers, including metal complexes, phthalocyanines, porphyrins and metal-free organic dyes, have been investigated and applied for DSSCs in the past decades.[2] Particularly, ruthenium complexes have received intensive interest due to their favorable photo-electrochemical properties and high stability.[3] So far several DSSCs based on ruthenium complexes have achieved photovoltaic efficiencies of over 10% under standard measurement conditions and the highest value being 11.5%.[4]

A great effort has been made to optimize the molecular structures of ruthenium complexes by changing ancillary ligands, typically bipyridines (*bpy*) or terpyridines(*tpy*), which can be tuned by different substituents (alkyl, aryl, heterocycle, etc.) to modulate their photochemical and photo-physical properties, and thus, improve the device photovoltaic performance.[5] Recently a novel class of thiocyanate free Ru(II) sensitizers with functionalized pyridyl azolate ancillary ligands has been reporrted, achieving high efficiencies over 10%. [6] It has been well-accepted that enhancing the molar extinction coefficient of sensitizer is an elegant strategy to improve the photovoltaic performance.[7] Incorporation high electron delocalization donor-antenna substituents into the ancillary ligands can substantially improve the light-harvesting property of such photo-sensitizers, therefore increasing the device overall power conversion efficiency (PCE).[8] Ruthenium complexes with ligands functionalized by carbazole-thiophenyl groups were well-designed to enhance the light-harvesting capacity, demonsting that carbazole moiety in the dye could enhance the performance of the device.[9] A series of heteroleptic ruthenium(II)-polypyridyl sensitizers were reported recently, in which electron-donating NMe_2 were changed to electron-withdrawing CN incorporated in the benzene-substituted bipyridine ligand.[10] The DSSC devices using these sensitizers have achieved efficiencies close to 10~11%. It has been demonstrated that by introduction electron-donor groups, such as triphenylamine (TPA), into the ancillary moieties, a positive charge or 'hole' can be shifted on to this moiety, potentially increasing the distance between the dye-cation moiety and the TiO_2 surface, and thus retarding the interfacial charge recombination dynamics.[11] Based on these strategies, several novel ruthenium dyes have been desiged and synthesized, whose ancillary bipyridine ligands are modified by a covalent attachment of triaryl amine-based electron donating groups.[12] DSSC devices utilized these dyes present relatively high PCEs in the range of 7~10%.[11] These sensitizer dyes exhibit not only efficient light harvesting capability, i.e., an extended absorption range and high molar absorption coefficient, but also an effective

intramolecular spatial charge separation of the excited-state of dye sensitizers, which are critically important for highly efficient DSSCs.

Herein we communicate an investigation on the influence of two electron-donating antennas upon the photo-physical and photo-electrochemical properties of ruthenium complexes and, especially, their photovoltaic performance in the DSSCs. Two new ruthenium sensitizers, coded as KW1 and KW2 (see Scheme 1), were designed and synthesized for this aim. For the KW1 dye molecule, the TPA is directly attached to the *bpy* unit, however, for the KW2 dye a thiophene used as the conjugated spacer incorporates between the TPA and *bpy* unit. The thiophene conjugated spacer has been demonstrated having a profound effect on the photo-physical properties of $[Ru(tpy)_2]^{2+}$ complexes because of its polarizability and low resonance energy.[13] We investigated their influence on DSSC devices performance. Especially, the interfacial charge transfer processes were investigated with transient phototovoltage/ photocurrent decay measurements together with electrical impedance analysis. Furthermore, for comparing the influences of the electron-donating groups on spectral and photovoltaic properties, we correlated these novel sensitizers with a model dye Z907[14], in which the aromatic amine electron donating groups is substituted by long alkyl chains.

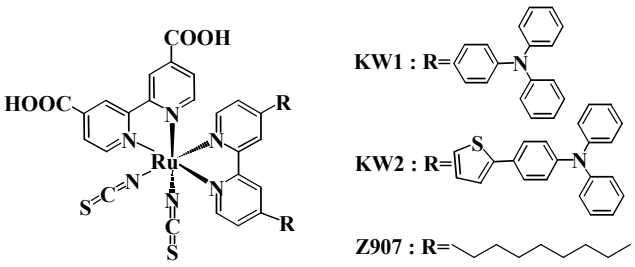

Scheme 1 Molecular structures of the ruthenium complex sensitizers KW1, KW2, and Z907.

Experimental Section

Materials and characterization: All solvents and reagents were of puriss grade quality and used as received except those specified. Dichloro(p-cymene) ruthenium (II) dimer and 4,4'-Dicarboxy-2,2'-bipyridine were purchased from Alfa Aesar. Ammonium thiocyanate and 3-phenylpropionic acid (PPA) were purchased from Aldrich. THF was dried with sodium sand and dimethylformamide (DMF) was distilled prior to use. 4,4'-Dibromo-2,2'-bipyridine,[15] 2-(4-(diphenyamino)-4,4,5,5-tetra methyl-1,3,2-dioxaborolane,[16] and N,N-diphenyl-4-(5-(4,4,5,5-tetramethyl-1,3,2-dioxaborolan-2-yl)thiophen-2-yl) aniline[17] were prepared according to the literature procedures.[3, 14] All reactions were performed under a dry argon atmosphere.

The structures of KW1 and KW2 were verified by NMR, MS, UV-vis spectroscopy and electrochemical measurement. ^{1}H NMR spectra were recorded on a Bruker AV400 400 MHz with tetramethylsilane as an internal standard. High resolution mass spectra (HRMS) were measured with a Bruker micro TOF mass spectrometer. Electronic absorption spectra were observed with a PE950 spectrophotometer and Fluorescent emission spectra were obtained with a Jasco FP-6500 spectrophotometer. Square-wave voltammograms of various dyes were measured on a CHI660C electrochemical workstation in a three-electrode single-compartment cell with a glassy carbon working electrode, a platinum wire counter electrode and an Ag/AgCl reference electrode. All potentials were internally referenced to the ferrocene/ferrocenium (Fc/Fc^+) couple.

*Synthesis of 4,4'-bis (N,N-diphenyl-4-aminophenyl)-2,2'-bipyridine (Ligand-**1**)*: A mixture of compound 2-(4-(diphenyamino)-4,4,5,5-tetramethyl-1,3,2-dioxaborolane (0.408 g, 1.1 mmol), 4,4'-Dibromo-2,2'-bipyridine (0.157 g, 0.5 mmol), and $Pd(PPh_3)_4$ (45 mg, 0.04 mmol) were dissolved in toluene/EtOH (2:1, v:v, 30 ml) and stirred for 10min. K_2CO_3 (1.1 g, 8 mmol) in 10 mL H_2O was subsequently added and the mixture was refluxed under argon for 40 h. After the mixture was cooled to room temperature, the organic layer was separated and the product was extracted with $CHCl_3$ (3×30 mL). The combined organic layers were dried with anhydrous Na_2SO_4 and the solvent was evaporated under reduced pressure. Purification of the crude product by column chromatography (CH_2Cl_2/hexane 1: 5) afforded Ligand-**1** as a yellow solid (0.170 g, yield 53%). ^{1}H NMR (400 MHz, $CDCl_3$, δ): 8.70 (s, 2H), 8.69 (d, J=5.2Hz, 2H), 7.68 (d, J=7.8Hz, 4H), 7.53 (d, 2H), 7.31-7.27 (t, J=7.5Hz, 8H), 7.17-7.14 (m, 12H), 7.06-7.09 (t, J=7.3Hz, 4H). MS (ESI) m/z calcd for ($C_{46}H_{34}N_4$): 642.79. Found: 643.4.

*Synthesis of 4,4'-bis(5-(N,N-diphenyl-4-aminophenyl)-thiophen-2-yl)-2,2'- bipyridine (Ligand-**2**)*: N,N-diphenyl-4-(5-(4,4,5,5-tetramethyl-1,3,2-dioxaborolan-2- yl) thiophen-2-yl) aniline (0.498 g, 1.1 mmol), 4,4'-Dibromo-2,2'-bipyridine (0.157 g, 0.5 mmol), K_2CO_3 (0.552 g, 4 mmol), and $Pd(PPh_3)_4$ (45 mg, 0.04 mmol) were dissolved in THF/H_2O (9:1, v:v, 50 ml). The solution was degassed and heated at reflux for 24 h upon which a half equivalent of $Pd(PPh_3)_4$ (22 mg, 0.019 mmol) was added to the reaction. The reaction was heated at reflux for another 16 h and then the product was extracted with $CHCl_3$ (3×30 mL). The combined organic layers were dried with anhydrous Na_2SO_4 and after the rotary evaporation of solvents, the resulting solid was purified by column chromatography on silica gel using 1:10 $CH_3OH/CHCl_3$ as an eluent to afford the target compound (0.194 g, 48% yield) as a yellow solid. ^{1}H NMR (400 MHz, $CDCl_3$, δ): 8.71 (d, J=5.3Hz, 2H), 8.69 (s, 2H), 7.65 (d, J=3.8Hz, 2H), 7.55 (m, 6H), 7.33-7.29(m, 10H), 7.17-7.07(m, 16H). MS (ESI) m/z calcd for ($C_{54}H_{38}N_4S_2$): 807.04. Found: 807.6.

*Synthesis of KW1 (Ru[(dcbpy)(ligand-**1**)(NCS)$_2$])*: Dichloro(p-cymene)ruthenium (II) dimer (0.11 g, 0.18 mmol) and ligand-**1** (0.231 g, 0.36 mmol) were dissolved in DMF (50 mL) and the solution was degassed. The reaction mixture was stirred at 75 °C for 4 h under Ar in the dark. Subsequently, 4,4'-dicarboxylic acid-2,2'-bipyridine (0.088 g, 0.36 mmol) was added and the reaction mixture was heated up to 145 °C for 4 h. Next, an excess of Ammonium thiocyanate (0.82 g, 10.80 mmol) was added to the resulting dark solution and it was continued for additional 4h at the same temperature. Then the reaction mixture was cooled to room temperature overnight. The solvent was removed on a roto-evaporator until little DMF remained and water (100 ml) was added to obtain a suspended solution. The resulting solid was collected on a sintered glass crucible by suction filtration, further washed with distilled water and diethyl ether, and dried under

vacuum. The crude product was dissolved in basic methanol (NaOH) and purified on a Sephadex LH-20 column with methanol as eluent. The main band was collected and the pH value of the collected solution was lowered to ca.3 by adding dilute HNO_3. The collected precipitate was washed with water and dried under vacuum. After purification, 0.167 g (yield 42%) of KW1 was obtained. ^{1}H NMR (400 MHz, DMSO-d_6 δ) 9.52 (d, J=5.8Hz, 1H), 9.21 (d, J=6.1Hz, 1H), 9.17 (s, 1H), 9.14 (s, 1H), 8.99 (s, 2H), 8.35 (d, J=5.6Hz, 1H), 8.29 (d, J=5.9Hz, 1H), 8.12 (d, J=8.6Hz, 2H), 7.95 (d, J=5.9Hz, 1H), 7.83 (d, J=5.2Hz, 2H), 7.68 (d, J=6.2Hz, 1H), 7.68-7.36 (m, 10H), 7.19-7.10 (m, 14H), 7.00-6.98 (d, J=8.4Hz, 2H). HRMS m/z calcd for ($C_{60}H_{42}N_8O_4RuS_2$) [M-NCS]$^+$, 1046.2062; found:1046.2069.

*Synthesis of KW2 (Ru[(dcbpy)(ligand-**2**)(NCS)$_2$])*: Subsequent to the one-pot synthesis described above for KW1, except for starting from Ligand-**2** (0.291 g, 0.36 mmol), The solvent was removed on a roto-evaporator until little DMF remained and water (100ml) was added to obtain a suspended solution. The insoluble solid was collected and washed intensively with water, further washed with diethyl ether and dried under vacuum. The black solid was dissolved in DMF and precipitated after addition of diethyl ether. This procedure was repeated twice and the product was obtained as a black solid. After purification, 0.155 g (yield 34%) of KW2 was obtained. ^{1}H NMR (400 MHz, DMSO-d_6 δ) 9.49 (d, J=5.6Hz, 1H), 9.18 (d, J=6.0Hz, 1H), 9.13 (s, 1H), 9.11 (s, 1H), 8.98 (s, 1H), 8.96 (s, 1H), 8.34 (d, J=5.8Hz, 1H), 8.30 (d, J=2.1Hz, 1H), 8.21 (d, J=5.3Hz, 1H), 8.10 (d, J=3.2Hz, 1H), 7.99-7.96 (m, 2H), 7.75-7. 71 (m, 3H), 7.65-7.59 (m, 4H), 7.42-7.32 (m, 9H), 7.15-7.05(m, 14H), 7.00-6.98(d, J=8.8Hz, 2H). HRMS m/z calcd for ($C_{68}H_{46}N_8O_4RuS_4$) [M-NCS]$^+$, 1210.1817; found: 1210.1760.

Device Fabrication: A screen-printed single or double layer film of interconnected TiO_2 particles was used as a mesoporous negative electrode. The 20-nm-sized TiO_2 particles were first printed on the fluorine-doped conducting glass (FTO) substrates and then coated with a 5-μm-thick second layer of 400-nm-sized light-scattering anatase particles (WER2-O, Dyesol) if needed. The film thickness was measured using a Profile-system (DEKTAK, VECCO, Bruker). The detailed preparation procedures of TiO_2 films have been described elsewhere. [4b] The TiO_2 film was first sintered at 500 °C for 30 min and then cooled to about 80 °C in air. Then the TiO_2 film electrodes were stained by immersing it into a dye solution containing KW1 or Z907 sensitizer (300 μM) in a mixture of acetonitrile and tert-butyl alcohol (volume ratio: 1/1) or a dye solution containing KW2 (300 μM) with 10% DMSO in acetonitrile and tert-butyl alcohol (volume ratio: 1:1) mixture overnight. After washing with acetonitrile and drying by air flow, the sensitized titania electrode were assembled with a thermally platinized FTO electrode. The electrodes were separated by a 45 μm thick hot melt ring (Surlyn, DuPont) and sealed by heating. The internal space was filled with a liquid electrolyte with use of a vacuum back filling system. In this study, a conventional liquid triiodide/iodide electrolyte (coded Z960) was used for high efficiency device, containing 0.1 M LiI, 0.05 M I_2, 0.6 M PMII, and 0.5 M 4-tert-butylpyridine in a mixture of valeronitrile and acetonitrile (volume ratio, 15: 85). A low volatility electrolyte was used for stability testing, containing 1.0 M DMII, 0.15 M I_2, 0.5 M N-butylbenzimidazole, and 0.1 M GNCS in methoxypropionitrile (MPN).

DSSC device characterization: A 450 W xenon light source solar simulator (Oriel, model 9119) with an AM 1.5G filter (Oriel, model 91192) was used to give an irradiance of 100 mW cm^{-2} (1 sun light intensity) at the surface of solar cells. The current-voltage characteristics of the cell were obtained by applying external potential bias to the sample and measuring the generated photocurrent with a Keithley model 2400 digital source meter (Keithley, USA). A similar data acquisition system was used to control the incident photon-to-current conversion efficiency (IPCE) measurement. A white light bias (1% sunlight intensity) was used to bring the total light intensity on the device under test closer to operating conditions. The devices with the photoanode area of 0.16 cm^2 were tested using a metal mask with an aperture area of 0.09 cm^2.

Electrochemical impedance spectroscopy and transient photovoltage decay measurements: Impedance measurements of DSSCs were carried out with an Autolab Frequency Analyzer set-up, which consists of an Autolab PGSTAT 30 (Eco Chemie B.V., Utrecht, The Netherlands) producing a small-amplitude harmonic voltage, and a frequency response analyzer module. The determination of the interfacial recombination rate constant was carried out by performing transient photovoltage decay measurements and charge extraction experiments. Details can be found in our previous report. [18]

Device Stability Test: The test was performed under illumination with visible light (1 sun; 100 mW cm^{-2}) at 60 °C, and the photovoltaic performance during the test was recorded. The physicochemical measurements were conducted at room temperature after the cell was equilibrated and cooled down to room temperature.

Results and Discussion

New ruthenium sensitizers coded as KW1 and KW2, which incorporate TPA- and TPA-thiophene-substituted bipyridines as the ancillary ligands, were synthesized with a stepwise synthetic protocol. The detailed synthesis procedures are illustrated in supporting information (Scheme S1). The desired disubstituted bipyridine ancillary ligands were obtained from the corresponding boronic acid with dibromopyridine by means of a Suzuki coupling reaction. The typical one-pot synthetic procedure developed for heteroleptic polypyridyl ruthenium complexes was employed for the preparation of the new sensitizers at a good yield.[14a] The detailed synthetic procedure for the new dyes and their identification with proton NMR (Figure S1 and Figure S2) and HRMS (Figure S3 and Figure S4), electronic absorption and emission spectroscopy (Figure 1) are described in the experimental section, which are found to be in good agreement with their structures.

The photo-physical and electrochemical properties of the KW1, KW2, and Z907 dyes were investigated and summarized in Table 1. Three absorption bands were observed in the 300-800 nm range both for the KW1 and KW2 dyes measured in DMF solution (Figure 1a, left ordinate). The intense absorption band around 300 nm are attributed to the intra-ligand π-π* charge transition of 4, 4'-dicarboxylic acid-2, 2'-bipyridine (dcbpy) and the ancillary bipyridine ligand. Another absorption band in UV

region is observed at 397 nm for the KW1 dye and 434 nm for the KW2 dye, which can be attributed to the π-π* transition of the ancillary bipyridine ligand and higher-energy metal-to-ligand charge transfer (MLCT) transition. The electronic absorption spectra of the KW1 and KW2 dyes present the characteristic MLCT absorption bands in the visible region, similar to other

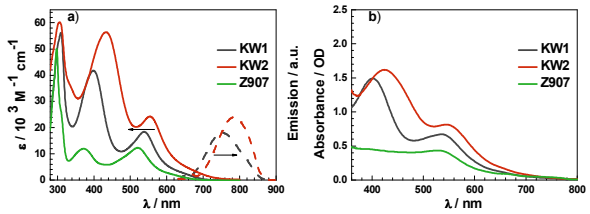

Fig. 1 a) Electronic absorption spectrum (left coordinate) of the KW1, KW2, and Z907 sensitizers dissolved in DMF and the emission spectrum (right coordinate) of KW1 and KW2. b) Electronic absorption spectrum of the KW1, KW2, and Z907 anchored on a 2.3-μm-thick mesoporous titania film.

Table 1 Absorption wavelength, fluorescence maxima and redox potentials of various ruthenium complex (KW1, KW2, and Z907) in DMF.

dye	λ_{abs} ($\varepsilon \times 10^3$ M^{-1} cm^{-1}) [a] [nm]	Emission[a] [nm]	E_{ox} [V] [b] vs. NHE	$E_{0\text{-}0}$ [eV] [c]	$E_{0\text{-}0^*}$ [eV] [d]
KW1	310 (56.2), 399 (41.7), 538 (18.4)	750	0.84	1.86	-1.02
KW2	307 (60.1), 392 (56.4), 554 (24.3)	785	0.90	1.78	-0.88
Z907	298 (50.1), 372 (11.9), 520 (12.0)	769 [e]	0.74 [e]	-	-

[a] Absorption and emission data were measured in DMF; [b] Recorded in DMF/0.1 M TBAP/N_2, GC working and Pt counter electrodes, Ag/AgCl reference electrode, scan rate = 50 mV s^{-1}; [c] The band-gap, $E_{0\text{-}0}$, was estimated from the intersection wavelengths of the normalized UV-vis absorption and the fluorescence spectra; [d] Excited-state oxidation potential was calculated according to the equation E_{ox}-$E_{0\text{-}0}$; [e] Z907 was synthesized according to reference [14a].

heteroleptic polypyridyl ruthenium (II) complexes.[19, 3c] In DMF, the lower energy MLCT band centred at 538 nm for the KW1 dye and 554 nm for the KW2 dye can be observed, which is 18 nm and 34 nm red-shifted compared to that of the reference Z907 dye, respectively. The molar extinction coefficients (ε) of the low-energy MLCT absorption bands for KW1 and KW2 were calculated to be 18.4×10^3 M^{-1} cm^{-1} and 24.3×10^3 M^{-1} cm^{-1}, respectively. These values are significantly higher than the Z907 model sensitizer (12.0×10^3 M^{-1} cm^{-1}) and the CYC-B6S sensitizer (16.1×10^3 M^{-1} cm^{-1}).[9a] The later has alkyl-substituted carbazole moieties in the thiophene-substituted bipyridine ligand.[9a] The molar extinction coefficient enhancement and bathochromic shift come from the extension π-conjugation in the ancillary ligand by incorporating electron-rich moieties.[20] Clearly, the DSSCs can be benefited from dyes with a high molar extinction coefficient. Consideration of a same surface area being occupied by sensitizers with different light harvesting efficiency, those with enhanced molar extinction coefficient allow to a high light harvesting yield, and eventually, a large reduction in film thickness. As shown in Figure 1b, the polypyridyl ruthenium (II) dyes containing TPA-donor antennas increased the visible light harvesting capacity due to a larger absorption cross section. This would fairly augment the device overall PCE because of reduced transport losses in the nanoporous environment for a thinner film.[12c] The molar absorption coefficients for the MLCT bands of KW1 and KW2 are much higher than those of analogous ruthenium complexes containing 5,5'-disubstituted-2,2'-bipyridine ancillary ligands (5,5'-bis(N,N-diphenyl-4-amino phenyl)-2,2'-bipyridine (6.4×10^3 M^{-1} cm^{-1}) and 5,5'-bis(5-(N,N-diphenyl-4-aminophenyl)-thiophen-2-yl)-2,2'-bipyridine (3.2×10^3 M^{-1} cm^{-1}).[21] This could be the main reason for the enhanced performance enhancement in devices with KW1 and KW2 dyes. The sensitizers display similar spectral features when adsorbed onto 2.3 μm transparent TiO_2 films, except for a slight blue shift of the absorption maxima due to interaction of anchoring groups to the surface.

The excitation of the low energy MLCT transitions of the KW1 or KW2 sensitizer in DMF solvent produces an emission maximum located at 750 or 785 nm (as shown in Figure 1a, right ordinate). Based on the absorption and emission spectra, the excitation transition energies ($E_{0\text{-}0}$) of the KW1 and KW2 dyes was evaluated to be 1.86 and 1.78 eV, respectively. Cyclic voltammetry measurements were performed in DMF solution using 0.1 M tetrabutylammonium hexafluorophosphate as the supporting electrolyte. The redox potentials [φ^0 (S^+ /S)] of the KW1 and KW2 sensitizers were estimated to be 0.84 and 0.90 V (vs. NHE, see Table 1). These are 0.34 and 0.4 V higher than that of the iodide electron donor (~0.5 V vs. NHE), providing sufficient driving force for dye regeneration. Furthermore, their excited state formal redox potentials [φ^0 (S^+/S^*)] were clculated to be -1.02 and -0.88 V (vs. NHE). The negative offset of [φ^0 (S^+/S^*)] relative to the conduction band edge of TiO_2 ensures the thermodynamic driving force for charge generation. The excited state potentials of the two dyes obtained in DMF are more negative than the conduction band of TiO_2, benefiting electron injection from these excited states to TiO_2.

Frontier molecular orbitals for KW1 and KW2 were calculated via the density functional theory (DFT) method in DMF at the cam-B3LYP/lanl2dz level with the Gaussian 09 package.[22] The HOMO and LUMO profiles of these two dyes are displayed in Figure 2. The HOMO of Z907 has essentially ruthenium t_{2g} character with sizable contribution coming from the NCS groups.[23] However, the HOMO of KW1 is delocalized partially over the NCS groups and TPA unit. In contrast, the HOMO of KW2 is located mainly on the TPA and thiophene moieties, resulting in an increased separation of the HOMO from the TiO_2 surface compared to Z907 and KW1. Apparently, the thiophene moiety can significantly tune the HOMO due to the enhanced electronic delocalization.

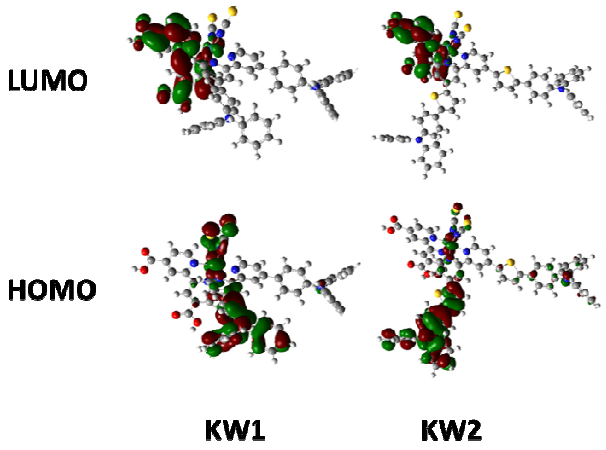

Fig. 2 The HOMO and LUMO for the KW1 and KW2 dyes from the DFT calculations (isodensity contour = 0.02 a.u.).

Some preliminary photovoltaic experiments were conducted to evaluate the performance of the new dyes employing transparent and double-layer titania films with different thicknesses. Initially, the transparent TiO_2 thin film (with the thick of 2.3 μm) were used to fabricate DSSCs, taking the advantage of the high optical cross section of the new dyes compared to Z907 sensitizer. These cells employed an a volatile acetonitrile-based electrolyte, containing 1.0 M 1,3-dimethylimidazolium iodide (DMII), 50 mM LiI, 30 mM I_2, 0.5 M tert-butylpyridine, and 0.1 M guanidinium thiocyanate (GNCS) in the mixed solvent of acetonitrile and valeronitrile (v/v, 85/15). [14c] Typical values for the photovoltaic parameters (open circuit voltage (V_{OC}), short circuit photocurrent density (J_{SC}) and fill factor (FF) of all three devices measured under 1 sun irradiation condition (the KW1 dye for device A, the KW2 dye for device B and the Z907 dye for device C) are summarized in Table 2. Encouragingly, device A (KW1 with TPA-substituted bipyridines) exhibited a V_{OC} of 0.764 V, a J_{SC} of 8.89 mA cm^{-2}, and a *FF* of 0.73, giving an overall PCE of about 5% when a 2.3 μm-thick TiO_2 film was used. Even with such a thin transparent titania film (2.3 μm), device B (the KW2 dye with TPA-thiophene-substituted bipyridines) exhibited a significant increase in the short circuit current density (J_{SC}= 11.24 mA cm^{-2}), yielding an overall PCE of 6.3% under illumination with standard AM 1.5G simulated sunlight (100 mW cm^{-2}). Under the same condition, the J_{SC} of device C (with the Z907 dye) was about 7.44 mA cm^{-2} and the PCE of device C (~4%) was less than two-thirds of device B. These results clearly revealed the advantages of the ruthenium dyes with high molar extinction coefficient for DSSC application.[10d,10e] This observation most probably stems from the superior molar extinction coefficient and the red shift in the absorption spectrum of KW2 dye relative to Z907 dye, which can be further verified from the corresponding incident photon-to-electron conversion efficiency (IPCE) spectra as exhibited in Figure S5.

Table 2 Detailed photovoltaic parameters of DSSC devices with the KW1, KW2, and Z907 sensitizers of varying film thickness in the presence and absence of PPA as co-adsorbent under full sunlight intensity.

Device	TiO_2 thickness [μm]	V_{OC} [V]	J_{SC} [mA cm^{-2}]	FF	PCE [%]
A (KW1)	2.3	0.764	8.89	0.73	4.98
B (KW2)	2.3	0.755	11.24	0.74	6.30
C (Z907)	2.3	0.758	7.44	0.71	4.05
D (KW1)	8.5+5	0.740	18.47	0.74	10.08
E (KW2)	8.5+5	0.725	18.90	0.74	10.07
F(Z907)	8.5+5	0.730	16.72	0.72	8.88
G (KW1+PPA)	8.5+5	0.767	18.63	0.74	10.64
H (KW2+PPA)	8.5+5	0.747	19.40	0.74	10.73

The competitive light absorption of triiodide from I^-/I_3^- redox couple could decrease the IPCE spectrum of a DSSC device at around 400 nm. [3d] In this work, there are strong absorption bands for the donor-antennas dyes with high molar extinction coefficient of about 44×10^3 M^{-1} cm^{-1} and 57×10^3 M^{-1} cm^{-1} at 397 nm for KW1 and 434 nm for KW2, which are significantly higher than those of Z907 dye (ε=10.9×10^3 M^{-1} cm^{-1}) and I_3^- (ε=25×10^3 M^{-1} cm^{-1}) at this wavelength.[3d] A large molar extinction coefficient in this region will offset the competitive visible light absorption due to I_3^- and recover the dip in the IPCE spectra around 400 nm. Actually, we found an obvious peak in this region in the IPCE spectra for KW1 and KW2-sensitized devices utilizing a thin film (with a thickness of 2.3 μm, Figure S5). It is noteworthy that devices A and B have an intensely increased IPCE response in the range of 400-450 nm.

The TiO_2 film thickness plays a vital role on the DSSC devices performance. To further explore the potential of these new dyes, solar cells were fabricated by using a double layer TiO_2 film (8.5 μm 20 nm sized TiO_2 transparent film with 5 μm 400 nm sized TiO_2 scattering layer) in conjunction with a volatile electrolyte (see experimental section) and with or without coadsorbent (3-phenylpropionic acid, PPA). Figure 3a presents the photocurrent density-voltage curves (*J-V*) characteristics of the devices based on these new donor-antenna sensitizers and Z907 dye, using the above mentioned volatile electrolyte under illumination with air mass (AM) 1.5 sunlight (100 mW cm^{-2}). The photovoltaic parameters of various devices are tabulated in Table 2. The device D (with the KW1 dye) had a J_{SC} of 18.47 mA cm^{-2}, a V_{OC} of 0.74 V, and a *FF* of 0.74, yielding an overall conversion efficiency of 10.08%. For the cell (device E) with the KW2 dye the corresponding device parameters (J_{SC}, V_{OC}, *FF*, and PCE) were 18.90 mA cm^{-2}, 0.725 V, 0.74, and 10.07%, respectively. Here we observed that for the device E with the KW2 dye the improvement in the short-circuit current was accompanied by a lower open-circuit voltage compared to KW1-sensitized device D. A reduced interfacial charge recombination in device E was also evident from the dark-current data for these devices (Figure S6), which addressed the voltage dependence of the recombination between the electrons in the TiO_2 and the electrolyte. The reduction in the dark current in device D relative to device E is consistent with the recombination dynamics as discussed below. In the presence of PPA as a coadsorbent (1:1 molar ratio in the dye staining solution), both the J_{SC} and V_{OC}

were increased for devices G and H (see Table 2), and conversion efficiency of 10.64% and 10.73% was achieved, respectively. This result can be attributed to the PPA was co-grafted with the dye molecules onto the surface of TiO_2 nanocrystals. The mixed dye/PPA monolayer appears to be more robust to impair the escape of photo-injected electrons into electrolytes.[24]

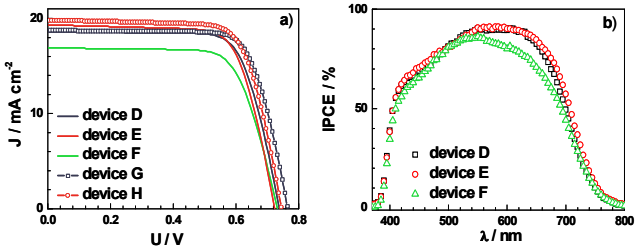

Fig. 3 a) J-V characterization for DSSC devices D (with the KW1 dye), device E (with the KW2 dye), device F (with the Z907 dye), device G (with the KW1 and PPA), and device H (with the KW2 and PPA) under AM 1.5G full-sunlight intensity. b) The photocurrent action spectra of DSSC devices D, E, and F, respectively.

The IPCE spectra of devices D (with the KW1 dye), E (with the KW2 dye) and F (with the Z907 dye) were illustrated in Figure 3b. The broad bands covered almost the entire visible spectrum from 450 nm to 700 nm with the maxima of 90%, 91% and 86% for devices D, E, and F, respectively. These results indicated that the increased J_{SC} values for device D and device E stemed from the higher IPCE response, which were attained a broad plateau of ~90% in the region around 600 nm. We can conclude that the substitution of donor-antennas for long alkyl chains improves the absorbed photon-to-current conversion efficiency and thus, its capacity to develop photon-generated charge.

The photovoltage of a DSSC is intrinsically determined by the potential difference between the quasi-Fermi level of TiO_2 and the redox potential of the electrolyte.[25] The V_{OC} can be affected by a shift of TiO_2 conduction band edge[26] as well as the degree of electron recombination reaction.[27] Unraveling of the details of the electron recombination dynamics between the photoinjected electrons at the TiO_2 and the oxidized electrolyte in various devices was undertaken by employing transient photovoltage measurements and charge-extraction measurements. Figure 4a illustrates the plot of the extracted charge density versus open circuit voltage for devices D, E, and F. The charge density was chosen as the abscissa in order to compare the V_{OC} values obtained from the three photoanodes at the same electron concentration in the dye-sensitized TiO_2 mesoporous films. The charge density for various dyes increased exponentially along with the increase of V_{OC}, which was generated by applying a gradually enhanced light intensity. This change in V_{OC} value can be explained qualitatively by a shift in the conduction-band edge (E_{cb}) with respect to the quasi-redox potential of the electrolytes. We observed that the conduction-band edge of the TiO_2 underwent an upward displacement in devices with compared to that of Z907. These energy shifts principally influence the devices' open-circuit voltage.[28] At an identical photo-induced charge density (1×10^{18} cm^{-3}), the photovoltage of device D (sensitized with the KW1 dye) was approximately 36 mV higher than that of F (sensitized with Z907 dye). It indicated that addition of TPA into ancillary ligand shifted the TiO_2 conduction band edge upward by about 36 mV, neglecting the change in the Nernst potential of the electrolyte. Figure 4b shows the recombination lifetime for various devices against the charge density. At a given charge density, the device F had the longest lifetime. This result indicated that the charge recombination was faster for devices D and E than for device F. Though the incorporation TPA- and TPA-thiophene-substituted bipyridines as the ancillary ligands increased the interfacial recombination as indicated in devices D and E, the effect was compensated by an increase in the conduction-band edge of the TiO_2 of these devices. These results indicated that different donor-antennas incorporated in the ruthenium sensitizers had an effect on the conduction band edge of TiO_2 as well as the recombination process at the same time.

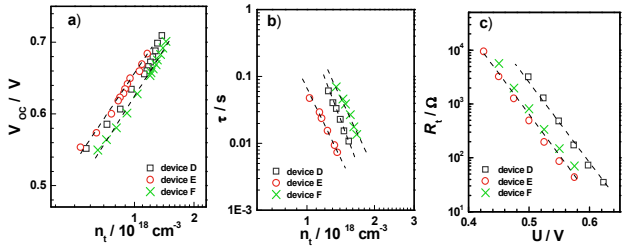

Fig. 4 Transient photovoltage decay measurements of the device D (with the KW1 dye), device E (with the KW2 dye), and device F (with the Z907 dye): a) the relationship between open circuit voltage and the photo-induced charge density and b) the relationship between recombination lifetime and the photo-induced charge density; c) electron transport resistance R_t of the TiO_2 film obtained from impedance measurement in the dark at 20 °C as a function of applied forward bias voltage for the devices.

Electronic impedance measurements (EIS) in dark were further performed to understand the differences in photovoltaic behavior of devices with various dye sensitizers. The impedance spectra for the DSSC devices (D, E, and F) revealed comparable characteristic information about the various kinetic processes. As presented in Figure 4c, the logarithm of the R_t shows parallel behavior for the three devices, which implies that the shift of the resistance for the steady state electron transport in these devices is caused by a change in position of the conduction band edge (E_{cb}).[14c] Presuming that electron mobility is the same among various devices, the TiO_2 conduction band edge energy level (E_{cb}) relative to the quasi-equilibrium potential for the redox couple can be determined by linear extrapolation of the experimental points in Figure 4c to their intersection with the abscissa. The R_t data from device D (sensitized with KW1) were shifted upward (~38 mV) from those of device F (Z907 used as sensitizer). Since the conduction band edge of the photoanode (dye coated TiO_2 film) is independent of the redox potential of electrolytes, the shift of the potentials in devices D and F can be attributed to a band edge modification[14c] induced by changing the molecular dipoles.[29] Clearly, the trend of the electron transport resistance of the various devices is well in agreement with that of the above

measured transient photovoltage decay values.

As discussed in the absorption spectroscopy, impedance and transient photovoltage investigations, these new donor-antennas sensitizers with different TPA-donor moieties have a beneficial influence on the conduction band edge energy levels of TiO_2 and light harvesting capability for the improvement of photovoltage and photocurrent. However, the electron recombination increases along with the large dimension of donor-antennas moieties compared to that bearing long alkyl chains. Thus, a high photovoltage would be expected in these devices with donor-antennas sensitizers if an efficient modification on the interface of TiO_2/dye was adopted. Actually, when a co-adsorbent (PPA) was added, an augment in photovoltage was obviously observed, showing high PCEs close to 11% (see Table 2). The KW2-sensitized device H provides a J_{SC} of 19.40 mA cm^{-2}, a V_{OC} of 0.744 V and a FF of 0.74, yielding an overall PCE of 10.73%.

A low volatility electrolyte (detailed compositions giving in the experimental section) based devices was used to evaluate the preliminary stability of the new sensitizers under moderate thermal stress and visible-light soaking. Both KW1 and KW2 showed similar behaviour during the stability testing. Figure 5 presents the representative variation in the photovoltaic parameters of KW2 sensitized cells when subjected to the accelerating test in a solar simulator at full sunlight (100 mW cm^{-2}) and 60 °C. The photovoltaic parameters, i.e., the V_{OC}, FF, J_{SC} and PCE of the fresh low volatility electrolyte based device with the KW2 dye were 0.69 V, 0.74, 18.4 mA cm^{-2}, and 9.29%, respectively. Over the 1000 hour light-soaking test period, the photovoltaic parameters J_{SC}, V_{OC}, FF, and PCE of the cell varied only slightly from the initial values. During the aging process, the value of the efficiency retained 95% of its initial value after 1000 hrs light soaking, a small drop of 46 mV in V_{OC} being compensated by an increase of 0.6 mA cm^{-2} in the J_{SC} values. Such an impressively stable performance implies the robustness of the KW2 dye itself as well as the dye sensitized heterojunction interface.

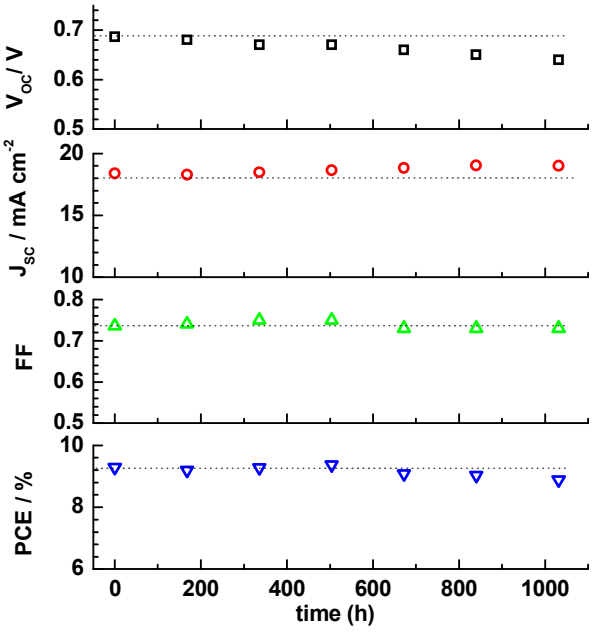

Fig. 5 Evolution of the photovoltaic parameters (J_{SC}, V_{OC}, FF and PCE) for the device based on (8.5+5) μm TiO_2 double layer film sensitized with KW2 in the presence of PPA (1:1 molar ratio) as a coadsorbent and low volatility of liquid electrolyte (with MPN solvent) during the visible light soaking (100 mW cm^{-2}) at 60 °C.

Conclusions

In summary, we have designed and synthesized two new heteroleptic ruthenium sensitizers with a feature of incorporating high electron delocalization TPA-donor antennas into the ancillary ligands. These new dyes exhibit remarkable light-harvesting capacities and the corresponding DSSC cells achieved impressive power-conversion efficiencies close to 11% under AM 1.5G simulated sunlight. The different spacer between bipyridyl and TPA-donor will clearly influence the photophysical and electrochemical properties of this class of ruthenium complexes as well as their interface behaviors on the TiO_2, which were scrutinized by impedance and transient photovoltage decay measurements. Based on these studies and findings, the photo-activity of ruthenium sensitizers containing donor-antennas can be successfully improved by careful molecular engineering.

Notes and references

[a] *Michael Grätzel Center for Mesoscopic Solar Cells, Wuhan National Laboratory for Optoelectronics, Huazhong University of Science and Technology, 1037 Luoyu Road, 430074 Wuhan, P. R. China, E-mail:mingkui.wang@mail.hust.edu.cn*

[b] *School of Materials Science and Engineering, Wuhan Textile University, FangZhi Road, 430073, Wuhan, P. R. China, E-mail: xujie0@mail.ustc.edu.cn*

[c] *Department of Materials Engineering, Monash University, Melbourne, Victoria, 3800, Australia*

† Electronic Supplementary Information (ESI) available: [Synthesis routs of ancillary ligands KW-Ll and KW-L2, and their NMR and HRMS characterization, and rark-current measurement]. See DOI: 10.1039/b000000x/

1 G. Vougioukalakis, A. Philippopoulos, T. Stergiopoulos, P. Falaras, *Coord. Chem. Rev.* **2011**, *255*, 2602.

2 a) J. Yina, M. Velayudham, D. Bhattacharya, H. Lin, K. Lu, *Coord. Chem. Rev.* **2012**, *256*, 3008; b) J. Clifford, M. Planells, E. Palomares, *J. Mater. Chem.* **2012**, *22*, 24195; c) L. Li, E. W. Diau, *Chem. Soc. Rev.* **2013**, *42*, 291; d) M. Liang, J. Chen, *Chem. Soc. Rev.* **2013**, *42*, 3453.

3 a) O. Kohle, M. Grätzel, A. Meyer, T. Meyer, *Adv. Mater.* **1997**, *9*, 904; b) F. Gao, Y. Wang, D. Shi, J. Zhang, M. Wang, X. Jing, R. Humphry-Baker, P. Wang, S. Zakeeruddin, M. Grätzel, *J. Am. Chem. Soc.* **2008**, *130*, 10720; c) Y. Cao, Y. Bai, Q. Yu, Y. Cheng, S. Liu, D. Shi, F. Gao, P. Wang, *J. Phys. Chem. C* 2009, 113, 6290; d) L. Han, A. Islam, H. Chen, C. Malapaka, B. Chiranjeevi, S. Zhang, X. Yang , M. Yanagida, *Energy Environ. Sci.* **2012**, *5*, 6057.

4 C. Chen, M. Wang, J. Li, N. Pootrakulchote, L. Alibabaei, C. Ngocle, J. Decoppet, J. Tsai, C. Grätzel, C. Wu, S. Zakeeruddin, M. Grätzel, *ACS Nano* **2009**, *3*, 3103.

5 A. Hagfeldt, G. Boschloo, L. Sun, L. Kloo, H. Pettersson. *Chem. Rev.* **2010**, *110*, 6595.

6 a) K. Wu, W. Ku, J. N. Clifford, E. Palomares, S. Ho, Y. Chi, S. Liu, P. Chou, M. K. Nazeeruddin, M. Grätzel, Energy Environ. Sci. 2013, 6, 859; b) S. Wang, K. Wu, E. Ghadiri, M. G. Lobello, S. Ho, Y. Chi, J. Moser, F. D. Angelis, M. Grätzel, M. K. Nazeeruddin, Chem. Sci. 2013, 4, 423.

7 P. Wang, S. M. Zakeeruddin, J. E. Moser, R. Humphry-Baker, P. Comte, V. Aranyos, A. Hagfeldt, M. K. Nazeeruddin, M. Grätzel, *Adv. Mater.* **2004**, *16*, 1806.

8 a) C. Chen, N. Pootrakulchote, S. Wu, M. Wang, J. Li, J. Tsai, C. Wu, S. M. Zakeeruddin , M. Grätzel. *J. Phys. Chem. C* **2009**, *113*, 20752; b) J. Yum, I. Jung, C. Baik, J. Ko, M. Nazeeruddin, M. Grätzel. *Energy Environ. Sci.* **2009**, *2*, 100; c) K. Willinger, K. Fischer, R. Kisselev, M. Thelakkat, *J. Mater. Chem.* **2009**, *19*, 5364; d) M. Wang, S. Moon, D. Zhou, F. Formal, N. Cevey-Ha, R. Humphry-Baker, C. Grätzel, P. Wang, S. Zakeeruddin, M. Grätzel, *Adv. Funct. Mater.* **2010**, *20*, 1821; e) A. Mishra, N Pootrakulchote, M. Wang, S. Moon, S. Zakeeruddin, M. Grätzel, P. Bäuerle, *Adv. Funct. Mater.* **2011**, *21*, 963.

9 a) C. Chen, J. Chen, S. Wu, J. Li, C. Wu, K. Ho, Angew. Chem. Int. Ed. 2008, 47, 7342; b) S. Fan, C. Kim, B. Fang, K. Liao, G. Yang, C. Li, J. Kim, J. Ko, J. Phys. Chem. C 2011, 115, 7747.

10 W. Han, J. Han, H. Kim, M. J. Choi, Y. Kang, C. Pac, S. O. Kang, Inorg. Chem. 2011, 50, 3271.

11 a) S. Haque, S. Handa, K. Peter, E. Palomares, M. Thelakkat, J. Durrant, *Angew. Chem. Int. Ed.* **2005**, *44*, 5740; b) N. Hirata, J. Lagref, E. Palomares, J. Durrant, M. Nazeeruddin, M. Grätzel, D. Censo, *Chem. Eur. J.* **2004**, *10*, 595.

12 a) C. Karthikeyan, H. Wietasch, M. Thelakkat. *Adv. Mater.* **2007**, *19*, 1091; b) H. Snaith, C. Karthikeyan, A. Petrozza, J. Teuscher, J. Moser, M. Nazeeruddin, M. Thelakkat, M. Grätzel, *J. Phys. Chem. C* **2008**, *112*, 7562; c) J. Yum, S. Moon, C. Karthikeyan, H. Wietasch, M. Thelakkat, S. Zakeeruddin, M. Nazeeruddin, M. Grätzel, *Nano Energy* **2012**, *1*, 6.

13 K. Robson, B. Koivisto, T. Gordon, T. Baumgartner, C. Berlinguette, *Inorg. Chem.* **2010**, *49*, 5335.

14 a) M. Nazeeruddin, S. Zakeeruddin, J. Lagref, P. Liska, P. Comte, C. Barolo, G. Viscardi, K. Schenk, M. Grätzel, *Coord. Chem. Rev.* **2004**, *248*, 1317; b) P. Wang, S. Zakeeruddin, J. Moser, M. Nazeeruddin,T. Sekiguchi, M. Grätzel, *Nat. Mater.* **2003**, *2*, 402; c) M. Wang, P. Chen, R. Humphry-Baker, S. Zakeeruddin, M. Grätzel, *ChemPhysChem* **2009**, *10*, 290.

15 H. Staats, F. Eggers, O. Haß, F. Fahrenkrug, J. Matthey, U. Lüning, A. Lützen, *Eur. J. Org. Chem.* **2009**, 2009, 4777.

16 B. Liang, L. Wang, Y. Xu, H. Shi, Y. Cao, *Adv. Funct. Mater.* **2007**, *17*, 3580.

17 S. Li, X. Yang, M. Cheng, J. Zhao, Y. Wang, L. Sun, *Tetrahedron* **2012**, *53*, 3425.

18 J. Lu, X. Xu, Z. Li, K. Cao, J. Cui, Y. Zhang, Y. Shen, Y. Li, J. Zhu, S. Dai, W. Chen, Y. Cheng, M. Wang, *Chem. Asian J.* **2013**, *8*, 956.

19 a) S. Zakeeruddin, M. Nazeeruddin, R. Humphry-Baker, P. Pechy, P. Quagliotto, C. Barolo, G. Viscard, M. Grätzel，*Langmuir* **2002**, *18*, 952; b) P. Wang, S. Zakeeruddin, J. Moser, R. Humphry-Baker, P. Comte, V. Aranyos, A. Hagfeldt, M. Nazeeruddin, M. Grätzel, *Adv. Mater.* **2004**, *16*, 1806.

20 Q. Yu, S. Liu, M. Zhang, N. Cai, Y. Wang, P. Wang, *J. Phys. Chem. C* **2009**, *113*, 14559.

21 F. Dai, W. Wu, Q. Wang, H. Tian, W. Wong, Dalton Trans. 2011, 40, 2314.

22 M. Frisch, G. Trucks, H. Schlegel, G. Scuseria, M. Robb, J. Cheeseman, G. Scalmani, V. Barone, B. Mennucci, G. Petersson, H. Nakatsuji, M. Caricato, X. Li, H. Hratchian, A. Izmaylov, J. Bloino, G. Zheng, J. Sonnenberg, M. Hada, M. Ehara, K. Toyota, R. Fukuda, J. Hasegawa, M. Ishida, T. Nakajima, Y. Honda, O. Kitao, H. Nakai, T. Vreven, J. Montgomery, J. Peralta, F. Ogliaro, M. Bearpark, J. Heyd, E. Brothers, K. Kudin, V. Staroverov, R. Kobayashi, J. Normand, K. Raghavachari, A. Rendell, J. Burant, S. Iyengar, J. Tomasi, M. Cossi, N. Rega, J. Millam, M. Klene, J. Knox, J. Cross, V. Bakken, C. Adamo, J. Jaramillo, R. Gomperts, R. Stratmann, O. Yazyev, A. Austin, R. Cammi, C. Pomelli, J. Ochterski, R. Martin, K. Morokuma, V. Zakrzewski, G. Voth, P. Salvador, J. Dannenberg, S. Dapprich, A. Daniels, O. Farkas, J. Foresman, J. Ortiz, J. Cioslowski, D. Fox, Gaussian Inc., Wallingford CT **2009**.

23 S. Handa, H. Wietasch, M. Thelakkat, J. Durrant, S. Haque, *Chem. Commun.* **2007**, *17*, 1725.

24 a) P. Wang, S. Zakeeruddin, R. Humphry-Baker, J. Moser, M. Grätzel, *Adv. Mater.* **2003**, *15*, 2101; b) P. Wang, S. M. Zakeeruddin, R. Humphry-Baker, M. Grätzel, *Chem. Mater.* **2004**, *16*, 2694.

25 D. Hagberg, J. Yum, H. Lee, F. Angelis, T. Marinado, K. Karlsson, R. Humphry-Baker, L. Sun, A. Hagfeldt, M. Grätzel, M. Nazeeruddin, *J. Am. Chem. Soc.* **2008**, *130*, 6259.

26 Z. Zhang, S. Zakeeruddin, B. O'Regan, R. Humphry-Baker, M. Grätzel, *J. Phys. Chem. B* **2005**, *109*, 21818.

27 a) A. Reynal, A. Forneli, E. Martinez-Ferrero, A. Sánchez-Díaz, A. Vidal-Ferran, B. O'Regan, E. Palomares, *J. Am. Chem. Soc.* **2008**, *130*, 13558; b) B. O'Regan, K. Walley, M. Juozapavicius, A. Anderson, F. Mata, T. Ghaddar, S. Zakeeruddin, C. Klein, J. Durrant, *J. Am. Chem. Soc.* **2009**, *131*, 3541.

28 a) E. Barea, J. Ortiz, F. Paya, F. Fernandez-Lazaro, F. Fabregat-Santiago, A. Sastre-Santos, J. Bisquert, *Energy Environ. Sci.* **2010**, *3*,1985; b) A. Allegrucci, N. Lewcenko, A. Mozer, L. Dennany,P. Wagner, D. Officer, K. Sunahara, S. Mori, L. Spiccia, *Energy Environ. Sci.* **2009**, *2*, 1069.

29 a) M. Wang, C. Grätzel, S. Moon, R. Humphry-Baker, N. Rossier-Iten, S. M. Zakeeruddin, M. Grätzel, *Adv. Funct.Mater.* **2009,** *19*, 2163; b) P. Chen, J. Yum, F. Angelis, E. Mosconi, S. Fantacci, S. Moon, R. Baker, J. Ko, M. Nazeeruddin, M. Grätzel, *Nano Lett.* **2009**, *9*, 2487; c) J. Krüger, U. Bach, M. Grätzel, *Adv. Mater.* **2000**, *12*, 447.